Three-Dimensional *SAR* Distributions Computed in a Multilayered Cylindrical Model for Electromagnetic Hyperthermia

STEVEN C. HILL, MEMBER, IEEE, AND DIPAKBIN Q. CHOWDHURY

Abstract—**A model consisting of multilayered, concentric, circular cylinders is used to numerically investigate specific absorption rate (*SAR*) distributions for electromagnetic hyperthermia. The fields in the cylinders are expanded in eigenfunctions, and axial confinement is achieved via Fourier transformation. Only axisymmetric *SAR* distributions are considered. TM_0 modes have *SAR* distributions appearing most useful for hyperthermia of deep-seated tumors. As the *SAR* is more confined axially: 1) the radial components of the TM_0 mode fields increase, and 2) the attenuation in the radial direction increases. Differences in *SAR* distributions are more apparent near the surface of a model than they are near the core. The effects of axial confinement on the optimal frequency of operation are discussed.**

I. Introduction

TEMPERATURE distributions generated using noninvasive electromagnetic (EM) applicators are often significantly worse than those thought best for hyperthermia therapy. Deep-seated tumors are particularly difficult to heat adequately [1]–[3], even with annular array applicators [4]–[6], which appear to be the most useful noninvasive devices for such tumors [7]–[10].

Both theoretical and experimental studies suggest that improved phasing of applicator arrays may in some cases provide improved specific absorption rate (*SAR*) [11]–[14] or temperature [9], [15], [16] distributions. Most of the mathematical models for such studies have been two-dimensional [11]–[14] and most of the optimization has been reported in 2-D models.

A small number of studies of 3-D *SAR* distributions have also been reported. Guy *et al.* [17] computed the fields generated by aperture applicators in multilayered circular concentric cylindrical (MCC) models. Only the fields in the $z = 0$ plane were reported, where z is the axial direction. Rappaport and Morganthaler [18], [19] optimized the computed *SAR* distributions in homogeneous cylindrical and spherical models. Cottis *et al.* [20] showed they could numerically improve the *SAR* distributions generated by concentric coil type applicators in MCC models. Hagman and Levin [21] computed the fields in a model of a man and found that the curvature and the finite length of the body are important for annular array type applicators. Paulsen *et al.* [10] computed the *SAR* distributions produced in homogeneous 3-D man models by annular array, capacitive plate, and concentric coil applicators. It is clear from these computations, from the measurements of Turner [5] and Samulski *et al.* [22], and from the arguments of Hagmann [21] that the 3-D nature of the body and the inhomogeneities of the body are important in determining the temperature distributions. However, it is at present difficult and costly to compute *SAR* distributions in models having arbitrary inhomogeneities in 3-D [24]. It is useful to first learn as much as possible using simpler models. A general solution for the fields generated in MCC models by aperture sources has been formulated by Wait [25].

We would like to determine the best achievable 3-D *SAR* distributions in a MCC model. In this paper we consider the *SAR* distributions of the modes, study the effects of axial confinement and type of axial confinement on the *SAR* distributions, and discuss the effect of axial confinement on the optimal operating frequency.

Significant features of the approach taken in this paper are as follows:

1) Only the fields internal to the body model are considered. The problem of applicator design can be considered later if improved *SAR* distributions are obtained. We chose this approach partly because it simplifies the analysis and because we do not want our determination of the optimum *SAR* distributions to be subject to the limitations of existing applicators.
2) MCC models are chosen because: a) 3-D *SAR* distributions can be computed with confidence in these models, b) these models can approximate some important inhomogeneities of the body, c) it is possible to think in terms of standard mode structures in these models, and d) the relative simplicity of the models allows us to focus on the optimization problem.
3) It is assumed that a desired *SAR* distribution in the model has already been specified to be axisymmetric

Manuscript received October 11, 1988; revised March 2, 1989. This work was supported by the National Science Foundation under Grant EET-8708687.

The authors are with the Department of Electrical and Computer Engineering, Clarkson University, Potsdam, NY 13676.

IEEE Log Number 8928322.

and at the center of the cylinder. We generally try to increase the *SAR* at the center while limiting the maximum *SAR* in other regions.

4) Since the MCC model is useful for studying the effects of confining the field in the axial direction these effects are emphasized here. Problems with 2-D analysis of annular array type applicators have been stated clearly by Hagmann [23]. Here the primary effects of axial confinement using TM modes, i.e., more rapid attenuation of the fields, and altered directions of the fields (radial fields when fields are primarily intended to be axial), are quantified for sample MCC models.

II. Methods

A. Computation of Fields in Multilayered Concentric Cylinders

Our method of solution is similar to Guy's [17] (see also the references cited in [25]). Our analysis differs from Wait's [27] in that we do not specify material outside the finite cylinder, our cylinder is layered, and we do not solve for the fields generated by aperture sources.

In our concentric cylindrical model the radius of the lth layer is ρ_l. The cylinder has a length L. The solution is only valid inside the cylinder between $\pm L/2$. Only the internal problem is solved. The problem external to the cylinder is not specified. Our notation and approach follow Harrington [28]. In each layer the TM potentials are expressed as

$$\psi^m = \left[A_l^m J_n(k_{\rho_l}\rho) + B_l^m Y_n(k_{\rho_l}\rho)\right] e^{jn\phi} e^{jk_z z} \tag{1}$$

and the TE potentials are

$$\psi^e = \left[A_l^e J_n(k_{\rho_l}\rho) + B_l^e Y_n(k_{\rho_l}\rho)\right] e^{jn\phi} e^{jk_z z} \tag{2}$$

where $J_n(k_\rho\rho)$ and $Y_n(k_\rho\rho)$ are cylindrical Bessel and Neumann functions of order n; A_l^m, B_l^m, A_l^e, and B_l^e are expansion coefficients for the TE and the TM field in layer l; and k_z and k_ρ are the wave propagation constants in the z and ρ directions, which are related to the medium propagation constants by

$$k_l^2 = \omega^2\mu_l\epsilon_l = k_{\rho_l}^2 + k_z^2 \tag{3}$$

where μ_l is the permeability and ϵ_l is the complex permittivity in layer l. An $e^{j\omega t}$ time variation is assumed. In the central region ($l=1$) the coefficients of the $Y_n(k_\rho\rho)$ must be zero to avoid infinite fields at the origin.

The TM fields are obtained from the potentials using

$$E_\rho = \frac{1}{j\omega\epsilon}\frac{\partial^2\psi^m}{\partial_\rho\partial z} \qquad H_\rho = \frac{1}{\rho}\frac{\partial\psi^m}{\partial\phi}$$

$$E_\phi = \frac{1}{j\omega\epsilon\rho}\frac{\partial^2\psi^m}{\partial\phi\partial z} \qquad H_\phi = -\frac{\partial\psi^m}{\partial\rho} \tag{4}$$

$$E_z = \frac{1}{j\omega\epsilon}\left(\frac{\partial^2}{\partial z^2} + k^2\right)\psi^m \qquad H_z = 0.$$

The TE fields are obtained similarly [28].

The tangential components of the electric and magnetic fields (E_z, H_z, E_ϕ, H_ϕ) are matched at the boundary between the l and $l+1$ layers to obtain

$$[M_l][a_l] = [M_{l+1}][a_{l+1}] \tag{5}$$

where the matrix for the lth layer is

$$[M_l] = \begin{bmatrix} -\dfrac{jk_{\rho_l}^2 J_n(k_{\rho_l}\rho_l)}{\epsilon_l\omega} & -\dfrac{jk_{\rho_l}^2 Y_n(k_{\rho_l}\rho_l)}{\epsilon_l\omega} & 0 & 0 \\ 0 & 0 & -\dfrac{jk_{\rho_l}^2 J_n(k_{\rho_l}\rho_l)}{\mu_0\omega} & -\dfrac{jk_{\rho_l}^2 Y_n(k_{\rho_l}\rho_l)}{\mu_0\omega} \\ \dfrac{jk_z n J_n(k_{\rho_l}\rho_l)}{\epsilon_l\omega\rho_l} & \dfrac{jk_z n Y_n(k_{\rho_l}\rho_l)}{\epsilon_l\omega\rho_l} & k_{\rho_l} J_l'(k_{\rho_l}\rho_l) & k_{\rho_l} Y_l'(k_{\rho_l}\rho_l) \\ -k_{\rho_l} J_l'(k_{\rho_l}\rho_l) & -k_{\rho_l} Y_l'(k_{\rho_l}\rho_l) & \dfrac{jk_z n J_n(k_{\rho_l}\rho_l)}{\mu_0\omega\rho_l} & \dfrac{jk_z n Y_n(k_{\rho_l}\rho_l)}{\mu_0\omega\rho_l} \end{bmatrix} \tag{6}$$

and the potential vector for the lth layer is

$$[a_l] = \begin{bmatrix} A_l^m \\ B_l^m \\ A_l^e \\ B_l^e \end{bmatrix}. \tag{7}$$

When matching fields at the interface between layers l and $l+1$, the radius of the lth layer, ρ_l, is used in both $[M_l]$ and $[M_{l+1}]$.

Once the propagation constant k_z and the magnitude and phase of the potential in any layer are specified the matrices are used to find the potentials in any other layer. The approach is similar to that of Massoudi *et al.* [29] for 2-D fields. It can be seen in (5) and (6) that the TE and TM fields are coupled except in two special cases: 1) $n=0$, i.e., the fields have no ϕ dependence; and 2) $k_z=0$, i.e., the fields have no z dependence and the problem is 2-D.

The *SAR* is defined as $\sigma|E|^2/(2d)$, where d is the density (g cm^{-3}) of the medium. Since the *SAR* is propor-

tional to EE^*, axisymmetric distributions can be obtained using any order number, n (since $e^{jn\phi}e^{-jn\phi}=1$), but cannot be obtained using combinations of modes having differing n. A combination of orders is required to obtain a ϕ-dependent *SAR*. In the results shown in this paper only one order n is used in any one figure. Hence, the *SAR* distributions are axisymmetric and only radial and axial *SAR* variations need be shown.

The Bessel and Neumann functions were computed using the method and computer code described by Mason [30]. To avoid the effects of round-off errors that occurred in computing the matrices and fields for large k_z the boundary conditions for the tangential E and normal displacement vector were checked at each layer for each k_z. The round-off errors are in part a consequence of the $J_n(k_\rho\rho)$ and $Y_n(k_\rho\rho)$ being very nearly complex conjugates of each other when $k_\rho\rho$ is large and complex. The fields were not included whenever the boundary conditions were not matched to within 0.005 percent. Since the fields having large k_z have very poor radial *SAR* distributions their contributions to a desirable *SAR* distribution should be very small if not negligible. For torso model 1 described in subsection II-C, the maximum value of k_z used was near 63 m^{-1} at 70 MHz.

B. Confinement of Fields in the Axial Direction

The *SAR* distributions of the individual modes described in subsection II-A are independent of z since $e^{jk_z z}e^{-jk_z z}=1$. *SAR* distributions having a z dependence are obtained by combining modes as

$$\psi(z)=\int_{-\infty}^{\infty}\psi(k_z)e^{jk_z z}dk_z. \tag{8}$$

We assume the k_z are real so that the fields will be valid for an infinite cylinder or for a finite length cylinder with no sources at the ends. The Fourier integral above is approximated as a discrete sum. Consequently, the resulting *SAR* distributions are periodic in z. However, we are concerned only with the fields and *SAR* inside the cylinder of length L and ignore the external fields. Since we try to minimize the *SAR* near the ends of the cylinder, the currents leaving the ends of the cylinder are also kept relatively small.

The $\psi(k_z)$ are obtained by Fourier transformation of a desired distribution $\psi^m(z)$ in the core. In the case of TM fields we first specify a desired $E_z(z)$ and then use (4) to obtain the desired $\psi(z)$. For a Gaussian distribution the product of the $1/e$ point in z and the $1/e$ point in k_z is 2. Hence to confine a Gaussian E field distribution to within a $1/e$ half-width of 0.2 m requires a k_z distribution with a $1/e$ point of 10 m^{-1}. Fig. 1 shows the real and imaginary parts of k_ρ as a function of k_z as computed using (3). The rate of attenuation in the radial direction increases rapidly as the phase angle of k_ρ increases. Since axial confinement requires increased k_z, which in turn requires an increased imaginary part of k_ρ, a 2-D analysis (which requires $k_z=0$) gives the best-case *SAR* distributions. Since the higher k_z have E fields that increase more rapidly in moving from the core to the surface, it is desirable to use the smallest k_z that are required for axial confinement. A Gaussian distribution has a minimum space–frequency bandwidth product, and will be emphasized here.

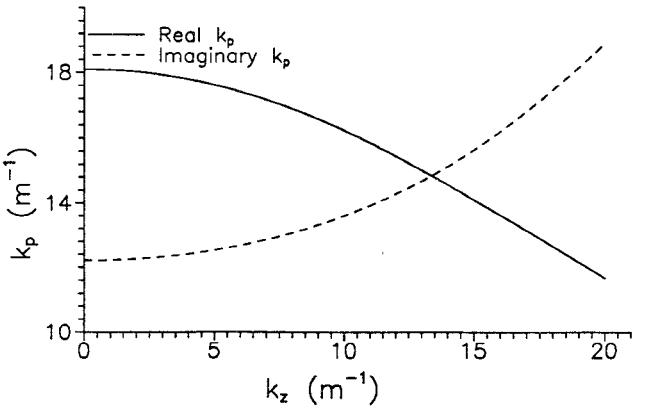

Fig 1. Effect of increasing k_z on the real and imaginary parts of k_ρ in muscle tissue (data in Table I) at 70 MHz.

C. Models

The permittivities and radii of the models are shown in Table I. The permittivity data are from [31] and [32]. Both models are approximations of a torso.

III. Results and Discussion

A. SAR Distributions for Modes That Are TE or TM in the Core

The radial distributions of *SAR* for torso model 1 with $k_z=10$ m^{-1} are shown in Fig. 2 for the two lowest-order TE and TM modes. In all figures the relative *SAR* is shown. It can be seen that with $k_z=10$ m^{-1} the best mode for depositing energy into the core of the layered cylinders is the TM_0 mode. The TE_1 mode is also nonzero at the core but has a large *SAR* in the fat layer. The dominant component of the TM_0 E fields in the core (the E_z) are directly proportional to $J_0(k_\rho\rho)$, which is nonzero at the origin. The TE_1 fields are proportional to $J_1(k_\rho\rho)/\rho$, which is also nonzero at the origin. The other Bessel functions are zero at the origin.

The electric fields of the TM_0 modes are primarily axially directed except in some fat or skin regions near the surface, and are the fields that could be preferentially excited by the annular array applicators [4] when all elements are excited with equal magnitude and phase. When the fields are not axisymmetric, higher order TM modes are required. The *SAR* distribution of the TE_1 mode would look better if the permittivities of the outer layers were larger. The electric fields of the TE_1 modes would be excited by a circular capacitive type applicator where the charge distribution on the capacitor varied as $\cos(\omega t-\phi)$. The usual capacitive type applicators would excite a variety of modes having differing n. In MCC models the TE_1 and higher order modes have the problem of large normal displacement, which can lead to overheating of low-permittivity regions [33]. The electric fields of the TE_0 modes

TABLE I
DESCRIPTION AND CONSTANTS FOR THE TORSO MODELS USED (M ≡ MUSCLE AND F ≡ FAT)

	model name	constitution	radial width (cm)	relative permittivity ϵ	conductivity σ S.m^{-1}	density gm.cm^{-3}
1.	Model 1	Muscle	0 - 4	83.0	0.80	1.02
		$\frac{1}{2}$ M + $\frac{1}{2}$ F	4 - 9	47.3	0.425	0.096
		M	9 - 11	83.0	0.80	1.02
		F	11 - 12	11.5	0.05	0.9
		$\frac{1}{3}$ M + $\frac{2}{3}$ F	12 - 13	35.3	0.300	0.94
		Water	13 - 15	78.0	0.0	1.0
2.	Model 2	M	0 - 13	83.0	0.80	1.02
		F	13 - 15	11.5	0.05	0.90

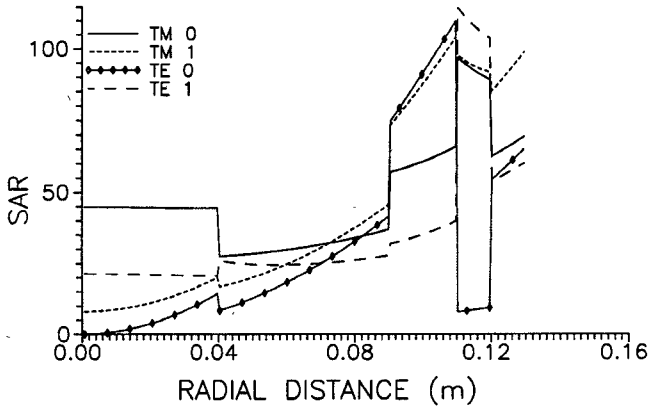

Fig. 2. Radial distribution of the relative *SAR* for $k_z = 10$ m^{-1} in torso model 1 at 70 MHz for differing TE and TM modes at $z = 0$.

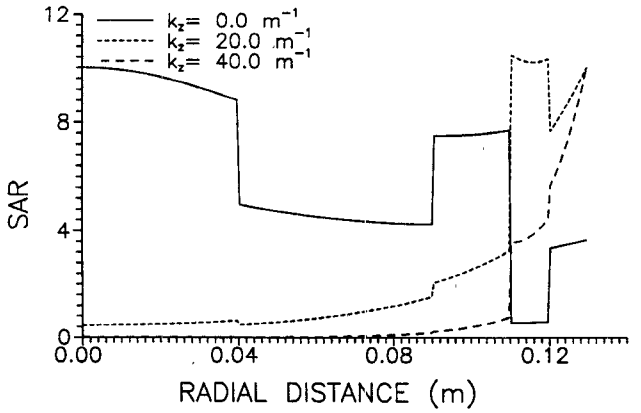

Fig. 3. Radial distribution of the relative *SAR* in torso model 1 at 70 MHz for differing k_z's. *SAR* calculated for the TM_0 mode at $z = 0$.

are ϕ directed, have a node at the origin as does $J_1(k_\rho\rho)$, and are the primary modes excited by concentric coil type applicators.

Since the TM_0 modes appear to have the best *SAR* distributions for hyperthermia of centrally located tumors, these modes will be emphasized here.

B. Effect of Axial Confinement on E Field and SAR Distributions

In a 2-D analysis the TM_0 electric fields are all axially directed and are continuous at the interfaces. The E fields are relatively constant, and the *SAR* distribution is primarily determined by the conductivity [7], [11].

To achieve axial confinement, modes having larger k_z and less desirable *SAR* distributions are required. In Fig. 3 the radial distributions of *SAR* for TM_0 fields are plotted for various values of k_z. It can be seen that as k_z increases the modes become less useful for hyperthermia of deep-seated tumors. Note that if the half-width of the E field distribution is to be 20 cm, then significant amplitudes of the Fourier coefficients of $k_z = 10$ to 30 m^{-1} are required.

As k_z increases the *SAR* becomes less useful for two reasons. First, the increased k_z causes an increase in the phase angle of k_ρ. Consequently, the magnitude of $J_0(k_\rho\rho)$ is a much more rapidly increasing function of ρ. Second, the radial electric fields increase rapidly as k_z increases, even for the axisymmetric TM_0 case. Radial fields are to be avoided near interfaces because the continuity of the normal displacement vector results in the overheating of low-permittivity (e.g. fat) tissues that share an interface with a high-permittivity (e.g. muscle) region [33]. That the radial fields increase with k_z can be seen in (4), and in the matrices (equation (6)) where the coupling between TE and TM modes is seen to be proportional to k_z.

The effects of axial confinement in two different torso models are considered next. Plots of *SAR* distributions are shown in Fig. 4 for TM_0 fields having three different distributions of E_z in the water just outside the skin layer. In Fig. 4(a) the half-width of the Gaussian, i.e., where E_z drops to $1/e$ of its value at the center, is 21 cm. This value was chosen to give values comparable to measured *SAR* distributions for one type of annular array applicator [5]. The fields in Fig. 4(b) are more confined axially, but the maximum *SAR*'s in the fat layer are larger. *SAR*'s for an E_z variation of $\cos(\pi z/50)$ for all z having absolute values less than 25 cm and zero elsewhere were also computed but are not shown here. The distributions were similar to those of Fig. 4(b) except that the peak intensity in the fat was shifted from 13 cm to 19 cm. In Fig. 4(c) the E_z just outside the skin layer is uniform for all $|z| < 21$ cm, and is zero otherwise. Such a uniform E_z variation has been assumed in two analyses of annular array applicators using 3-D models [10], [21].

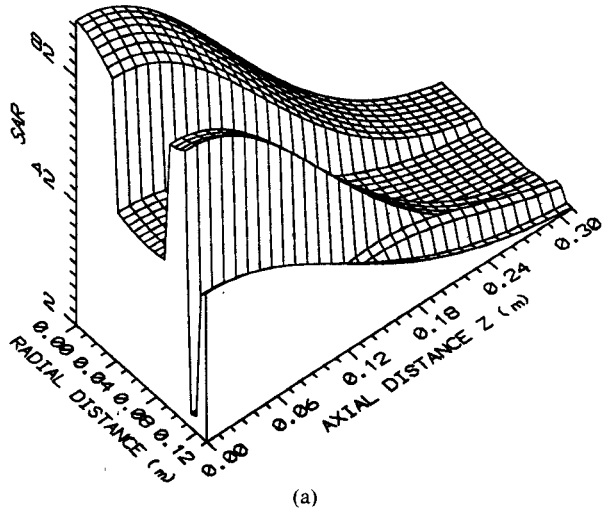

(a)

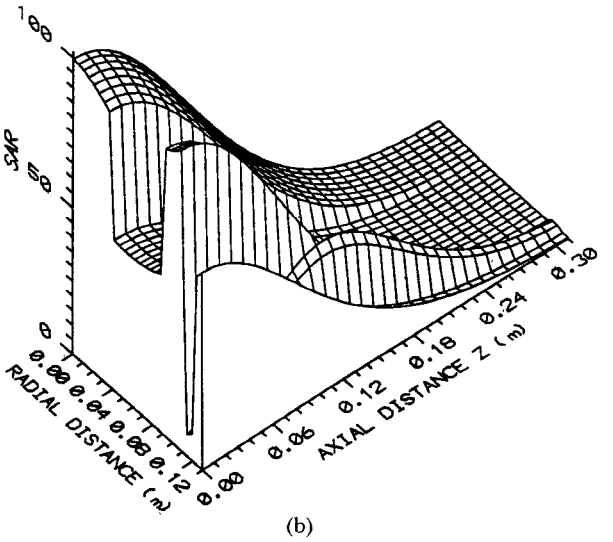

(b)

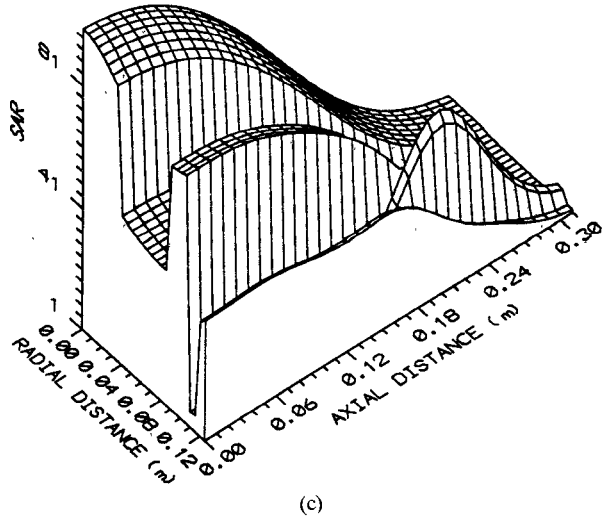

(c)

Fig. 4. Relative SAR in the $\rho-z$ plane of torso model 1 at 70 MHz. The Gaussian half-width for E_z is 21 cm in (a) and 14 cm in (b). In (c) E_z at the surface is uniform for all z within 21 cm of the center.

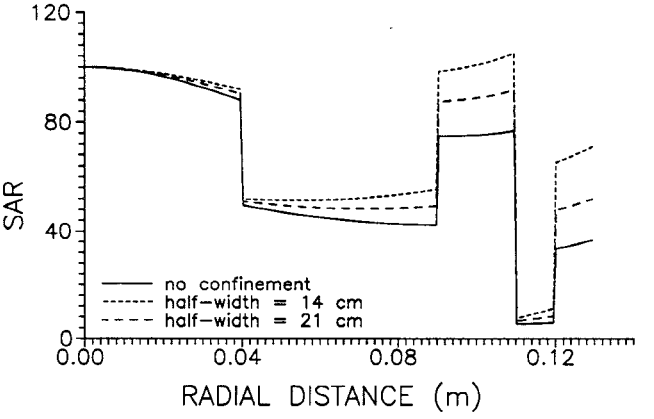

Fig. 5. Radial dependence of the the relative SAR in torso model 1 at 70 MHz with $z = 0$. The Gaussian half-widths for E_z are 0 (no axial confinement), 14 cm, and 21 cm.

In Fig. 4(a), (b), and (c) the differences near the surface are much more apparent than are the differences nearer the core. The E fields are essentially low-pass filtered in going from the surface to the core since the fields having higher k_z are more rapidly attenuated. When the E_z has a Gaussian distribution (Fig. 4(a)) the maximum SAR in the fat is several times smaller than when E_z is uniform (Fig. 4(c)). The relatively large SAR's in the fat layer 10 to 30 cm from the center are attributable to the radial E fields which are antisymmetric about $z = 0$. As can be seen in (4), when E_z is symmetric, E_ρ is antisymmetric. The SAR is nonzero at $z = 0$ because E_z, although smaller, is nonzero. Relative to muscle, the fat has a lower product of specific heat and density and it has a lower thermal conductivity [34]. Hence, the increased SAR in the fat may cause a significant increase in temperature. Burns in subcutaneous fatty tissues are occasionally observed in treatments with annular arrays [22]. Thermal modeling would help determine how significant the temperature rises are. In the rest of this paper only Gaussian distributions are assumed for E_z.

The effects of axial confinement on the radial SAR distribution are shown more clearly in Fig. 5, where the SAR versus radius is plotted at $z = 0$ for Gaussian half-widths of infinity (no axial confinement), 21 cm, and 14 cm. Again, the more confined fields have poorer radial SAR distributions. Since the maximum SAR in fat occurs at a nonzero z, the SAR at the fat layer appears better than it is. An annular array applicator in which the axial distribution of the field could be controlled might have advantages for hyperthermia.

The effects of axial confinement on the radial E fields are shown in Fig. 6. The lengths of the arrows are proportional to the amplitudes of the fields. The half-width of the Gaussian in E_z at the surface is 21 cm. In comparing with other figures (not shown) we have found that as the fields are more confined the field lines exit the muscle over a shorter distance, and the magnitudes of the radial E vectors in the fat increase.

The effects of axial confinement on the electric field and SAR distributions are next shown for torso model 2, which

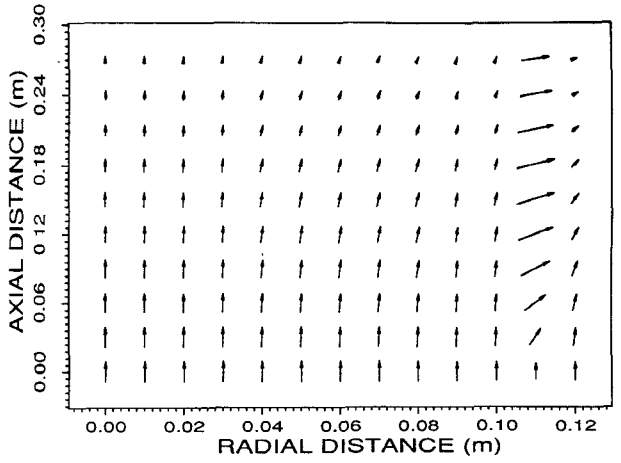

Fig. 6. Vector E field plots for torso model 1 at 70 MHz. The Gaussian half-width for E_z at the outer surface is 21 cm. Only the real part of E, i.e., E at $t = 0$, is plotted.

consists of homogeneous muscle surrounded by a homogeneous layer of fat. This model is chosen because temperatures measured during simulated treatment of the model with an annular array have been reported [22]. The model is shown in Fig. 7(a), where the positions x_1 and x_2 are indicated. The parameters are given in Table I. Since Samulski *et al.* [22] measured the rise in temperature, we computed the temperature rise, assuming no thermal diffusion, by dividing the *SAR* by the specific heat. The z dependence of our computed temperature rise at $\rho = x_1$ and $\rho = x_2$ is shown in Fig. 7(b) and (c). The curves in Fig. 7(b) are generally consistent with the experimental results; Samulski *et al.* [22] measured relatively large increases in the temperature of the fat layer away from the $z = 0$ plane. The *SAR* corresponding to the antisymmetric E_ρ has peaks at $z = \pm 16$ cm in Fig.7(b) and at $z = \pm 12$ cm in Fig. 7(c). With less axial confinement the E_ρ and double peaks in the fat decrease.

C. Frequency Effects

Torso model 2 was also used to study the effects of frequency on the computed temperature rise in the fat, assuming no thermal diffusion. The computed temperature rise in muscle and fat near the muscle–fat interface is plotted versus frequency in Fig. 8(a) and (b). The radial positions for the temperature plots are taken at the points of maximum temperature in the fat and muscle near the interface. The temperature rise in each figure is normalized to a 4° rise in the center of the model. In Fig. 8(b) the maximum temperature in the muscle occurs at $z = 0$ and the maximum temperature in the fat occurs between 14.5 and 17.5 cm from the center.

Note that when there is no axial confinement (Fig. 8(a)) the lower frequencies have lower computed maximum temperatures in the muscle and fat near the muscle–fat interface. In this 2-D analysis the lower frequencies appear to be more useful for hyperthermia of centrally located tumors. When the fields are confined as in Fig. 8(b), the computed increases in the temperatures in the fat are large at the lower frequencies.

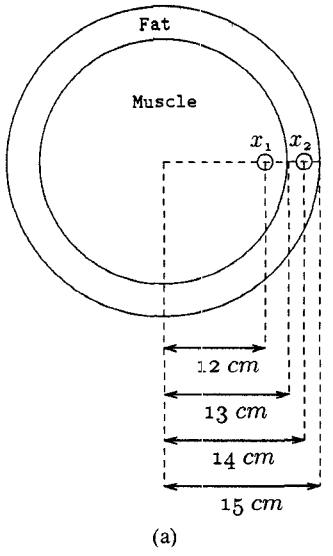

(a)

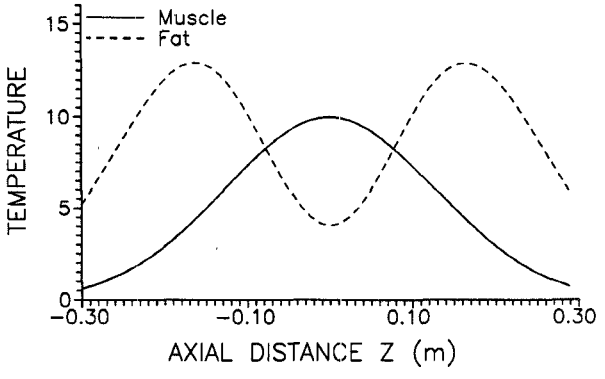

(b)

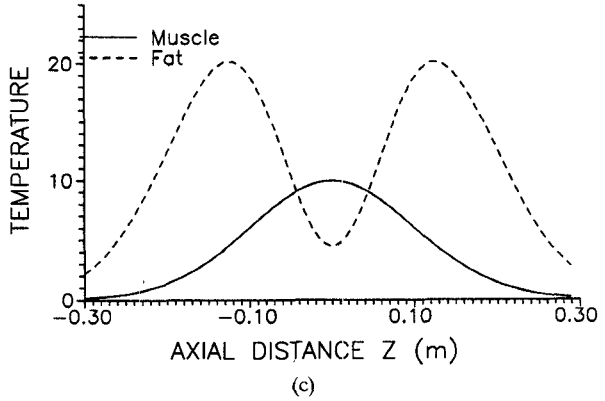

(c)

Fig. 7. Computed temperature rise versus z in torso model 2 for the TM_0 mode at 70 MHz. (a) Model showing the points $\rho = x_1$ and $\rho = x_2$. The temperature in muscle is at $\rho = x_1$ and in fat is at $\rho = x_2$. The Gaussian half-width for E_z is 21 cm in (b) and 14 cm in (c). The specific heat of muscle and fat used are 0.86 cal·g^{-1}·°C^{-1} and 0.24 cal·g^{-1}·°C^{-1} respectively.

IV. Summary

Aspects of the problem of finding the best *SAR* distributions in multilayered circular concentric cylindrical models of the human body are considered. We chose MCC models because they are inhomogeneous models in which 3-D *SAR* distributions can be computed accurately.

The primary findings for MCC models of the torso are as follows.

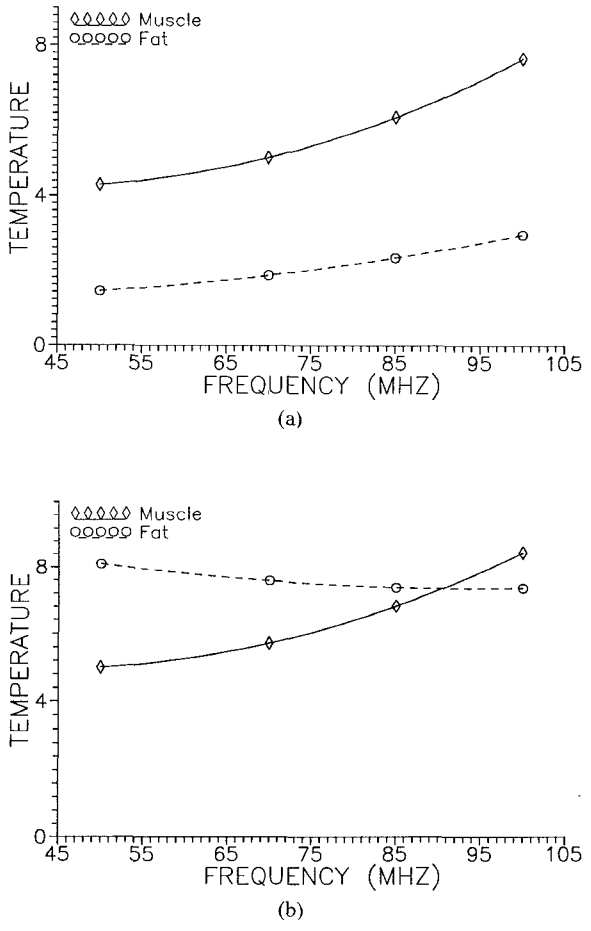

Fig. 8. Maximum temperature in the muscle and fat layers in torso model 2 as a function of frequency. (a) No axial confinement ($k_z = 0\ \mathrm{m}^{-1}$) (b) Gaussian half-width in E_z is 21 cm.

1) The TM_0 mode appears best for the hyperthermia of centrally located tumors. The TE_1 modes also deposit energy into the center of the model but do not have *SAR* distributions as useful as the TM_0 modes.

Items 2)–5) refer to TM_0 modes.

2) As the *SAR* distribution is confined axially, it also increases more rapidly with the radial distance from the center. This is because axial confinement requires larger k_z, which results in k_ρ being larger and having a larger phase angle. Hence the Bessel functions are more rapidly increasing functions of radial distance.
3) As the *SAR* distribution is axially confined the radial E fields increase, particularly in low-permittivity (e.g., fat) regions near the surface. These radial electric fields are antisymmetric. The resulting *SAR* distributions in the fat have maxima that are typically 15 to 25 cm above and below the $z = 0$ plane. The magnitudes of the maxima in the fat increase with axial confinement.
4) Differences between *SAR* distributions are more apparent near the surface than near the core. This is because the fields having larger k_z are more rapidly attenuated. The fields are essentially low-pass filtered as they move toward the core.
5) The maxima in the fat layer decrease with increasing frequency, in the range of 40 to 100 MHz, when the fields are confined with an E_z having a Gaussian half-width of 21 cm.

The computer codes developed here may be useful in assessing the accuracy of codes developed for field computations in arbitrary geometries. The codes are available to anyone who requests them.

References

[1] D. S. Shimm, T. C. Cetas, J. R. Oleson, J. R. Cassady, and D A. Sim, "Clinical evaluation of hyperthermia equipment: The University of Arizona institutional report for the NCI hyperthermia equipment evaluation contract," *Int. J. Hyperthermia*, vol. 4, no. 1, pp. 39–51, 1988.
[2] D. S. Kapp *et al.*, "Stanford University institutional report. Phase I evaluation of equipment for hyperthermia treatment of cancer," *Int. J. Hyperthermia*, vol. 4, no. 1, pp. 75–115, 1988.
[3] M. D. Sapozink, F. A. Gibbs, Jr., P. Gibbs, and J. R. Steward, "Phase I evaluation of hyperthermia equipment—University of Utah institutional report," *Int. J. Hyperthermia*, vol. 4, no. 1, pp. 117–132, 1988.
[4] P F. Turner, "Regional hyperthermia with an annular phased array," *IEEE Trans. Biomed.* Eng., vol. BME-31, pp. 106–114, 1984.
[5] P. F. Turner, "Hyperthermia and inhomogeneous tissue effects using an annular phased array," *IEEE Trans. Microwave Theory Tech.*, vol. MTT-32, pp. 874–882, 1984.
[6] P. F. Turner, "Mini-annular phased array for limb hyperthermia," *IEEE Trans. Microwave Theory Tech.*, vol. MTT-34, pp. 508–513, 1986.
[7] K. D. Paulsen, J. W. Strohbehn, and D. R. Lynch, "Theoretical thermal dosimetry produced by an annular phased array-type system in CT-based patient models," *Radiat. Res.*, vol. 100, pp. 536–552, 1984.
[8] K. D. Paulsen, J. W. Strohbehn, and D. R. Lynch, "A theoretical analysis of the benefits of amplitude and phase control for an annular array hyperthermia system for cancer therapy," in *Proc. 11th Ann. Bioeng. Conf* (Worcester, MA), 1985, pp. 74–77.
[9] J. W. Strohbehn, E. H. Curtis, K. D. Paulsen, X. Yuan, and D. R. Lynch, "Optimization of the absorbed power distribution for an annular phased array hyperthermia system," *Int. J. Radiat. Oncol. Biol. Phys.*, vol. 16, pp 589–599, 1989
[10] K D. Paulsen, J. W. Strohbehn, and D. R. Lynch, "Theoretical electric field distribution produced by three types of regional hyperthermia devices in a three-dimensional homogeneous model of man," *IEEE Trans. Biomed. Eng.*, vol. BME-35, pp. 36–45, 1988.
[11] V. Sathiaseelan, M. F. Iskander, G. C. W. Howard, and N. M. Bleehen, "Theoretical analysis and clinical demonstration of the effect of power pattern control using the annular phased-array hyperthermia system," *IEEE Trans. Microwave Theory Tech.*, vol. MTT-34, pp. 514–519, 1986.
[12] See the Special Issue on Phased Arrays for Hyperthermia Treatment of Cancer, *IEEE Trans. Microwave Theory Tech.*, vol. MTT-34, May 1986.
[13] J. R. Wait and M. Lumori, "Focused heating in cylindrical targets —Part II," *IEEE Trans. Microwave Theory Tech.*, vol. MTT-34, pp. 357–359, 1986.
[14] N. Morita, T. Hamasaki, and N. Kumagi, "An optimal method in multi-applicator systems for forming a hot zone inside the human body," *IEEE Trans. Microwave Theory Tech.*, vol. MTT-34, pp. 532–538, 1986.
[15] C. De Wagter, "Optimization of simulated two-dimensional temperature distributions induced by multiple electromagnetic applicators," *IEEE Trans. Microwave Theory Tech.*, vol. MTT-34, pp. 589–596, 1986.
[16] G. Arcangeli *et al.*, "Focusing of 915 MHz electromagnetic power on deep human tissue: A mathematical model study," *IEEE Trans Biomed. Eng.*, vol. BME-31, pp. 47–52, 1984.

[17] H. S. Ho, A. W. Guy, R. A. Sigelmann, and J. F. Lehmann, "Microwave heating of simulated human limbs by aperture sources," *IEEE Trans. Microwave Theory Tech.*, vol. MTT-19, pp. 224–231, 1971.
[18] C. M. Rappaport and F. R. Morganthaler, "Optimal source distribution for hyperthermia at the center of a sphere of muscle tissue," *IEEE Trans. Microwave Theory Tech.*, vol. MTT-35, pp. 1322–1327, 1987.
[19] C. M. Rappaport and F. R. Morganthaler, "Localized hyperthermia with electromagnetic arrays and leaky-wave throughguide applicator," *IEEE Trans. Microwave Theory Tech.*, vol. MTT-34, pp. 636–642, 1986.
[20] P. G. Cottis, N. K. Uzunoglu, and G. E. Chatzarakis, "A multiloop applicator with enhanced penetration depth," *IEEE Trans. Microwave Theory Tech.*, vol. 36, pp. 676–681, 1988.
[21] M. J. Hagmann and R. L. Levin, "Aberrant heating: A problem in regional hyperthermia," *IEEE Trans. Biomed. Eng.*, vol. BME-33, pp. 405–411, 1986.
[22] T. V. Samulski, D. S. Kapp, P. Fessenden, and A. Lohrbach, "Heating deep seated eccentrically located tumors with an annular phased array system: A comparative clinical study using two annular array operating configurations," *Int. J. Radiat. Oncol. biol. Phys.*, vol. 13, pp. 83–94, 1987.
[23] M. J. Hagmann, "Difficulties in using two-dimensional models for calculating the energy deposition in tissues during hyperthermia," *Int. J. Hyperthermia*, vol. 3, pp. 475–476, 1987.
[24] D. M. Sullivan, D. T. Borup, and O. P. Gandhi, "Use of finite-difference time-domain method in calculating EM absorption in human tissues," *IEEE Trans. Biomed. Eng.*, vol. BME-34, pp. 148–157, 1987.
[25] J. R. Wait, "General solution for excitation by slotted aperture source in conducting cylinder with concentric layering," *IEEE Trans. Microwave Theory Tech.*, vol. MTT-35, pp. 321–325, 1987.
[26] J. R. Wait, "General cylindrical model for focussed power deposition from an external antenna system," *J. Electromagnetic Waves and Applications*, vol. 2, no. 1, pp. 77–84, 1987.
[27] J. R. Wait, "Excitation of an enclosed lossy cylinder by an aperture source," *IEEE Trans. Microwave Theory Tech.*, vol. MTT-35, pp. 210–212, 1987.
[28] R. Harrington, *Time-Harmonic Electromagnetic Fields*. New York: McGraw-Hill, 1961, ch. 5.
[29] H. Massoudi, C. H. Durney, P. W. Barber, and M. F. Iskander, "Electromagnetic absorption in multilayered cylindrical models of man," *IEEE Trans. Microwave Theory Tech.*, vol. MTT-27, pp. 825–830, 1979.
[30] J. P. Mason, "Cylindrical Bessel functions for a large range of complex arguments," *Comput. Phys. Commun.*, vol. 30, pp. 1–11, 1983.
[31] C. H. Durney *et al.*, *Radiofrequency Radiation Dosimetry Handbook*, 2nd. ed. Salt Lake City, UT: The University of Utah, 1978.
[32] D. R. Lynch, K. D. Paulsen, and J. H. Strohbehn, "Finite element solution of Maxwell's equations for hyperthermia treatment planning," *J. Comput. Phys.*, vol. 58, pp. 246–269, 1985.
[33] D. A. Christensen and C. H. Durney, "Hyperthermia production for cancer therapy: A review of fundamentals and methods," *J. Microwave Power*, vol. 16, no. 2, pp. 89–105, 1981.
[34] K. D. Paulsen, J. W. Strohbehn, and D. R. Lynch, "Comparative theoretical performance for two types of regional hyperthermia system," *Int. J. Radiat. Oncol. Biol. Phys.*, vol. 9, pp. 1659–1671, 1985.

✠

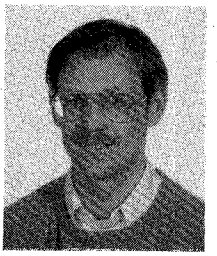

Steven C. Hill (S'82–M'85) received the B.S. degree in chemistry and the M.S. and Ph.D. degrees in electrical engineering from the University of Utah in 1973, 1982, and 1985, respectively. He also received the M.S. degree in pharmacology from Yale University, New Haven, CT, in 1977.

He is an Assistant Professor of Electrical and Computer Engineering at Clarkson University, Potsdam, NY. His research interests include hyperthermia, optical scattering by small particles, and nonlinear optics.

✠

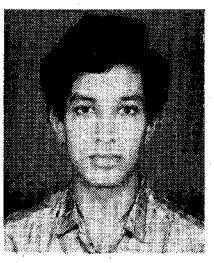

Dipakbin Q. Chowdhury was born in Bangladesh on January 1, 1964. He received the B.Sc. degree in electrical and electronic engineering from Bangladesh University of Engineering and Technology, Dhaka, Bangladesh, in 1986. Since September 1987 he has been a research assistant and then teaching assistant at Clarkson University, Potsdam, NY, where he is currently completing work for the M.S. degree in electrical engineering. His present research interest is in optimizing the *SAR* distribution in human tissue models for hyperthermia.